# High emission quantum yield $Tb^{3+}$-activated organic-inorganic hybrids for UV-down-shifting green light-emitting diodes

Sandra F. H. Correia,[a] Ricardo L. Fernandes,[a] Lianshe Fu,[a,b] Mariela M. Nolasco,[b] Luís D. Carlos[a] and Rute A. S. Ferreira*[a]

**Abstract:** Solid-state light-emitting diodes (LEDs) are driving the lighting industry towards efficient and environmentally friendly lighting and displays. Current challenges encompass efficient and low-cost down-shifting phosphors with tuned emission colors. Green light lies on the low-loss optical transmission window in plastic optical fibers, and plays a special role in human and plants circadian rhythm regulation. Moreover, green-emitting phosphors may suppress the 'green gap' found in semiconductor-based LEDs. In this work, a UV-photostable green-emitting complex, $Tb(NaI)_3(H_2O)_2$, with NaI= nalidixic acid (1-ethyl-1,4-dihydro-7-methyl-4-oxo-1,8-naftiridine-3-carboxylic acid), was incorporated into tripodal organic-inorganic hybrid materials. The hybrid hosts boost the absolute emission quantum yield from ~0.11 (isolated complex) to ~0.82 (doped hybrid), being the largest value reported for $Tb^{3+}$-based hybrid phosphors. A green-emitting LED was fabricated by coating a near-UV LED (365 nm) with a $Tb^{3+}$-activated organic-inorganic hybrid showing pure-green light with Commission International de l'Eclairage color coordinates and an efficacy value of (0.33, 0.59) and 1.3 $lm \cdot W^{-1}$, respectively.

## Introduction

Looking at the advancements in solid-state lighting over the last decade, lighting industries turned to the new emerging technology of the white light-emitting diodes (WLEDs) as they can achieve reduced energy costs for general indoor and outdoor lighting comparing with that of conventional solutions.[1] WLEDs can also be used in displays of variable sizes from large electrical billboards to small mobile phone displays due to their low dimensions and weight.

Current commercialized WLEDs rely on blue GaN-based LED chips covered with green-yellow phosphors, such as cerium-doped yttrium aluminum garnet ($YAG:Ce^{3+}$),[2] [3] whose main disadvantages are poor color-rendering index (CRI) and low stability of correlated color temperature (CCT).[4] A light bulb with tunable CRI and CCT can be attained by combining efficient red, green and blue (RGB) monochromatic emitting LEDs and adjusting their intensity fractions,[5] which reveals the importance of producing pure monochromatic color emitting devices.

The green light, in particular, is very important corresponding to the low-loss optical transmission window in plastic optical fiber (~500 nm)[6] and the most sensitive color for human eye response, playing a special role in the human and plants circadian rhythm regulation.[7] Moreover, improving green LED efficiency is also relevant to suppress the so-called 'green gap' which refers to the drastic fall of efficiency in semiconductor-based green-emitting LEDs.[8] An alternative approach to overcome the "green gap" is the combination of near-UV emitting LEDs and down-shifting phosphors able to efficiently convert the near-UV radiation from GaN-based LEDs into green light.[9]

Complexation of lanthanide ($Ln^{3+}$) ions with organic ligands has been extensively applied to develop efficient phosphors for LED applications, given the intrinsic pure and tunable emission colors of the ions. The judicious choice of the ligands requires high-absorption coefficients in the UV spectral region and efficient intramolecular energy transfer to the $Ln^{3+}$ excited states.[7i, 10] An efficient strategy to sensitize $Ln^{3+}$ ions is through the usage of a chromophoric molecule to generate an antenna effect.[11] The nalidixic acid (NaI, 1-ethyl-1,4-dihydro-7-methyl-4-oxo-1,8-naftiridine-3-carboxylic acid) is a weak monoprotic acid with a $pK_a$ value of 7.56. When coordinating $Ln^{3+}$ ions, the deprotonated NaI (nalidixate) is bound through the α-ketocarboxy group, acting as a bidentate ligand.[12]

In this work, a UV-photostable green-emitting complex, $Tb(NaI)_3(H_2O)_2$ (Figure 1), was incorporated into organic-inorganic tripodal hybrid materials with two average molecular weights (3000 and 5000 $g \cdot mol^{-1}$, termed as t-U(3000)[13] and t-U(5000), respectively) enabling an easy shaping and processing (fabrication of monoliths or films with controlled thickness). Moreover, the hybrid hosts boost the $Tb^{3+}$ green absolute emission quantum yield from ~0.11 in the isolated $Tb(NaI)_3(H_2O)_2$ complex to ~0.82 in the hybrid. A green-emitting prototype was successfully fabricated by coating a commercial near-UV LED (365 nm) with the $Tb^{3+}$-based organic-inorganic hybrids showing stable and pure-green light with Commission International de l'Eclairage (CIE) coordinates and an efficacy value of (0.33, 0.59), and 1.3 $lm \cdot W^{-1}$, respectively.

[a] Dr. S. F. H. Correia, R. L. Fernandes, Dr. L. Fu, Prof. L. D. Carlos, Prof. R. A. S. Ferreira
Physics Department and CICECO - Aveiro Institute of Materials, University of Aveiro, 3810-193 Aveiro, Portugal
E-mail: rferreira@ua.pt
URL: http://www.ciceco.ua.pt/RuteAndre
[b] Dr. M. M. Nolasco, Dr. L. Fu
Chemistry Department and CICECO - Aveiro Institute of Materials, University of Aveiro, 3810-193 Aveiro, Portugal

Supporting information for this article is given via a link at the end of the document.

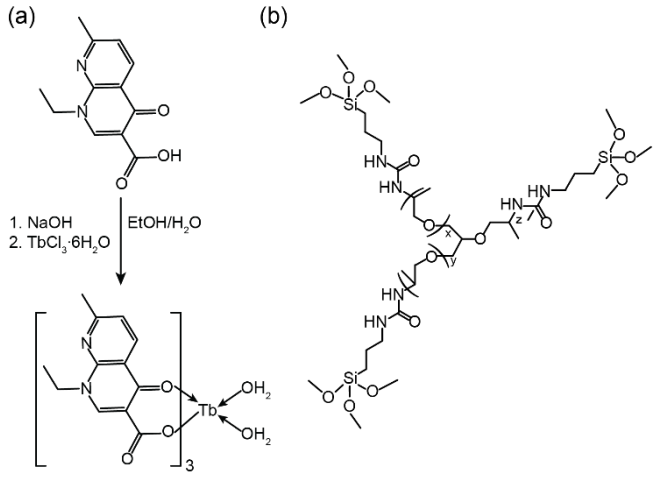


Figure 1. Schematic of the synthesis of (a) the $Tb(NaI)_3(H_2O)_2$ complex. (b) Representation of the molecular structure of the non-hydrolyzed precursors, t-UPTES(5000) (x+y+z≈85) and t-UPTES(3000) (x+y+z≈50).

## Results and Discussion

### Structural characterization

A comparison between the FT-IR and Raman spectra of the pristine host, t-U(5000), and of the $Tb^{3+}$-based hybrids, tU5Tb is provided by Figure 2. Similar information was obtained for the low-average molecular weight materials (t-U(3000) and tU3Tb), Figure S6).

The medium-to-weak intensity FT-IR band at 927 $cm^{-1}$ provides evidence that in tri-ureasils the polyoxyethylene chains attain complete disorder and the medium intensity peak at 1014 $cm^{-1}$ is attributed to the strongly coupled vibrations of $CH_2$ rocking, and C-O and C-C stretching modes. The most intense FT-IR band, attributed to the C-O stretching mode, is found at 1106 $cm^{-1}$ and the broad envelope bands with maxima at 1251 and 1375 $cm^{-1}$ are related to $CH_2$ twisting and wagging modes, respectively. Concerning the polyether backbone Raman signatures in the 2700-3100 $cm^{-1}$ region in Figure 2, the t-U(5000) spectra present three narrower intense bands at 2871, 2933 and 2973 $cm^{-1}$, assigned to the $CH_2$ symmetric and asymmetric and $CH_3$ asymmetric stretching υ-C-H modes, respectively.

The “amide II” mode, a mixture of C-N and C-C stretching modes and in-plane bending mode of N-H group, is located at 1567 $cm^{-1}$ and does not change when $Tb(NaI)_3(H_2O)_2$ complex is incorporated. For the “amide I” vibration, a highly complex vibration associated essentially with the C=O stretching mode,[14] although the profile of the band maxima at 1644 $cm^{-1}$ remains unchanged, the shoulder at 1720 $cm^{-1}$ is intensified. The incorporation of the $Tb(NaI)_3(H_2O)_2$ complex into the hybrid matrix disturbs the “amide I” region leading to a band redistribution. This suggests that the coordination ability of the hybrid host is strong enough to replace water molecules from the $Tb^{3+}$ first coordination sphere by carbonyl groups of the urea moieties, which agrees with the photoluminescence results (as will be discussed later). A complex broad feature centered at *ca* 3342 $cm^{-1}$ covers the entire 3200-3450 $cm^{-1}$ region of the spectra of all the hybrids (Figure S7). This band is related with the superposition of the stretching vibration of the hydrogen-bonded N−H groups of the urea bridges, residual silanol groups, and adsorbed water[15] preventing, therefore, the detection of any spectral changes attributed to the replacement of the two water molecules of the $Tb^{3+}$ complex.

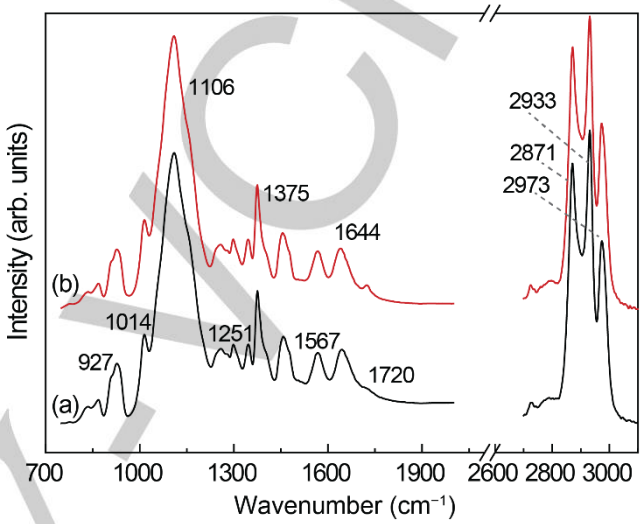


Figure 2. FT-IR (700-2000 $cm^{-1}$) and Raman (2700-3100 $cm^{-1}$) spectra of (a) t-U(5000) and (b) tU5Tb.

Aiming at studying the effect of the materials processing through spin-coating in the local-structure, the hybrid films were also studied by attenuated total reflectance (ATR) and Raman spectroscopies (Figure S8 and S9). All spectra show an overall similar profile dominated by the strong and broad bands of the host tri-ureasil materials. It should be noted, however, that the materials processing through spin-coating are accompanied by a change in the intensity of the “amide” vibrations at 1565, 1640 and 1722 $cm^{-1}$ relative to the total spectrum. The possibility of a structure with a lower degree of the organization may be the explanation to that.

### Optical properties

The ability of the hybrids to absorb UV radiation was inferred from the spectral dependence of the absorption coefficient, as illustrated in Figure 3 and Figure S10 for selected materials.

We note the high molar absorption coefficients in the UV for the ligand (~$2x10^4$ $M^{-1}\cdot cm^{-1}$, NaI) and of the isolated $Tb^{3+}$-based complex (~$2x10^5$ $M^{-1}\cdot cm^{-1}$), Figure S10. The spectrum of the tU5Tb hybrid processed as monolith reveals a broadband in the UV spectral range (225-325 nm), also detected in the non-doped hybrid and similarly to that already measured for analogous di-ureasil-based materials.[17] The presence of a low-relative intensity band in the high-wavelength region (325-375 nm) is also detected only for the $Tb^{3+}$-containing materials and is ascribed to the low-lying singlet state ($S_1$, 335 nm) of the NaI ligands (Figure S10). We note that the contribution of the high-energetic singlet state ($S_2$, 257 nm) of the NaI ligand cannot be ruled out as it overlaps the hybrid host excited states (Figure S10). We notice

that the excitation spectra of the films are blue-shifted when compared with that of the monolithic samples, as already observed for other sol-gel derived hybrid materials and it was ascribed to differences in the gelification and condensation rates between the spin-coating process in the film and the sol-gel reactions in the monoliths.[18] In the case of films, the forced solvent extraction is much faster, compared with that of bulk monoliths, resulting in a structure with a lower degree of organization (as Raman and ATR spectroscopies pointed out, Figure S8 and S9).

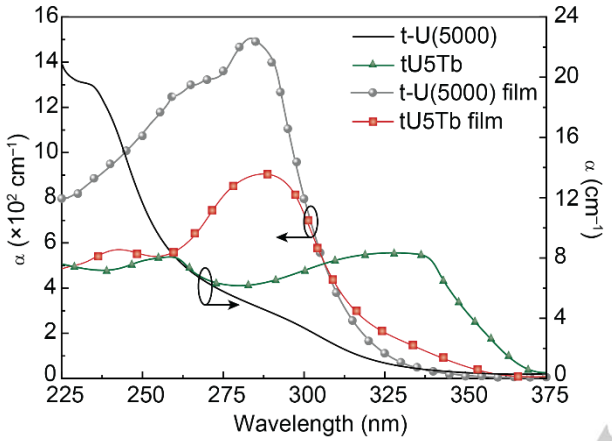


Figure 3. Absorption spectra of the t-U(5000) and of the tU5Tb processed as monoliths and as films.

Under UV/Vis excitation the $Tb^{3+}$-based hybrids display a green emission visible to the naked eyes, already detected for the isolated complex, Figure 4. The green emission results from the $Tb^{3+}$ $^5D_4 \rightarrow {}^7F_{6\text{-}0}$ transitions (Figure 4b) and is independent of the excitation wavelength (Figure S12), suggesting that in each sample the $Tb^{3+}$ ions occupy the same average local environment. Nevertheless, we note that the energy of the Stark component changes after the complex incorporation, pointing out an effective interaction with the hybrid host. The fact that no emission arising from the ligands is observed suggests an efficient ligands-to-$Tb^{3+}$ energy transfer.[19] Moreover, we note that the intrinsic emission[13a] from the pristine t-U(5000) and t-U(3000) (Figure S13 and S14) is also absent in the spectra of the tU5Tb hybrids indicating that the excited states of the hybrids are also active in the energy transfer processes.[19]

The presence of energy transfer between the ligands/hybrid excited states and the $Tb^{3+}$ levels is also discerned in the excitation spectra monitored within the $^5D_4 \rightarrow {}^7F_5$ transition (Figure S15). The excitation spectra reveal two main components at 280 and 362 nm ascribed to the ligands' singlet excited states also observed in the absorption spectra of the hybrid samples (Figure 3) and of the isolated complex (Figure S10 and S11). The spectra of the complex and of the hybrid also reveal the presence of a very low-relative intensity intra-$4f^8$ transition ascribed to the $^7F_6 \rightarrow {}^5D_4$ transition. The negligible relative intensity of this transition points out that the $Tb^{3+}$ excited states ions are mainly populated via the ligands, rather than by direct intra-$4f^8$ excitation. For the materials prepared as films, the excitation spectra (Figure S14b) resembles that of the monoliths, except for the red-shift of the ligands excited states, as already noticed by absorption spectroscopy.

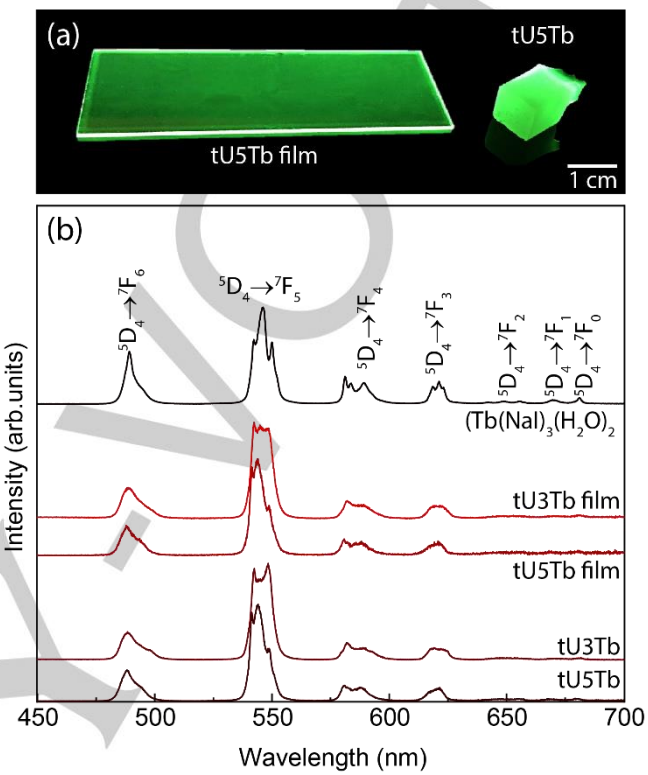


Figure 4. (a) Photographs of the tU5Tb processed as film and monolith under UV excitation (365 nm). (b) Emission spectra (300 K) excited at 275 nm of $Tb(NaI)_3(H_2O)_2$ complex and of the tU5Tb and tU3Tb processed as monoliths and films.

To further discuss the effect of the $Tb(NaI)_3(H_2O)_2$ complex incorporation into the hybrid host on the $Tb^{3+}$-local coordination the photoluminescence data were acquired at low-temperature for the $Tb(NaI)_3(H_2O)_2$ complex, tU5Tb and tU3Tb (Figure S16). After complex incorporation, we note that despite the same number of Stark components for the $Tb^{3+}$ $^5D_4 \rightarrow {}^7F_{6\text{-}0}$ transitions is observed, changes are noticed in the energy and relative intensity, which confirms that the $Tb^{3+}$ local coordination was affected by the incorporation into the hybrid host. The $Tb^{3+}$ local-coordination emission properties were also studied by the measurement of the $^5D_4$ emission decay curves (Figure S17-S19). For the $Tb(NaI)_3(H_2O)_2$ complex and the hybrids processed as monoliths the same measurements were also performed at 18 K (Figures S18-S20).

All the $^5D_4$ emission decay curves are well described by a single-exponential function, in good agreement with the presence in each sample of a single average $Tb^{3+}$-local environment. The $^5D_4$ lifetime values ($\tau$), resulting from the best fits to the decay curves (Figures S17-S22), are listed in Table 1. The $^5D_4$ lifetime values of the hybrid samples (monoliths and films) are higher than those measured for $Tb(NaI)_3(H_2O)_2$ complex reinforcing that

changes occurred in the $Tb^{3+}$ coordination shell after the incorporation into the hybrid hosts. The lifetime variation may be rationalized attending to the fact that the experimental transition probability may be expressed as $\tau^{-1} = \tau_r^{-1} + \tau_{nr}^{-1}$, where $\tau_r^{-1}$ and $\tau_{nr}^{-1}$ represent the radiative and non-radiative transition probabilities, respectively, and that at low-temperature $\tau^{-1} \sim \tau_r^{-1}$.[20] Thus, as the temperature is raised, the decrease in $\tau$, suggests that the non-radiative mechanisms ($\tau_{nr}^{-1}$) are larger for the isolated $Tb(NaI)_3(H_2O)_2$ complex than after its incorporation into the hybrid. This evidence supports that the two labile water molecules present in $Tb(NaI)_3(H_2O)_2$ complex are released and replaced by the oxygen atoms of the carbonyl groups from the urea linkages in hybrid materials, as reported for other $Ln^{3+}$-based ureasils.[21] We also note that the similarity between the $^5D_4$ lifetime values of the monoliths and films reinforces that the $Tb^{3+}$-local environment is not affected by the processing and, therefore, the blue-shift of the absorption and excitation spectra observed for the films compared with the analogous monolith hybrids is related to changes beyond the $Tb^{3+}$-first coordination sphere.

**Table 1.** $^5D_4$ lifetime values ($\tau$, $\pm 0.01\times10^{-3}$ s) measured at 18 K and 300 K for the $Tb(NaI)_3(H_2O)_2$ complex and the hybrid materials.

| | | monoliths | | films | |
|---|---|---|---|---|---|
| T (K) | $Tb(NaI)_3(H_2O)_2$ | tU5Tb | tU3Tb | tU5Tb | tU3Tb |
| 18 | 0.95 | 1.07 | 1.08 | - | - |
| 300 | 0.69 | 1.11 | 1.11 | 1.10 | 1.08 |

The emission properties of the materials were further quantified through quantum yield measurements, Table S1. We notice the significant enhancement of the absolute emission quantum yield after the complex incorporation, in line with the replacement of the water molecules in the $Tb^{3+}$ first coordination sphere. An analogous effect was already reported for $Eu^{3+}$-based aqua-complexes after incorporation into analogous hybrid materials.[21] Moreover, we note that the maximum emission quantum yield of tU5Tb processed as a monolith (0.82 excited at 365 nm) is the largest one reported for $Tb^{3+}$-based hybrids. Another relevant property is the emission stability under UV radiation. Contrarily to that typically found in organic-based complexes,[22] the typical photobleaching observed in the initial irradiation time interval is not detected for the $Tb(NaI)_3(H_2O)_2$ complex (Figure S23).

**UV-down-shifting green-emitting LED**

Attending to the larger quantum yield of tU5Tb it was selected to fabricate a UV-down-shifting green-emitting LED device by coating commercial ultraviolet LED chips emitting at 365 nm (Figure 5), which presented calculated CIE 1931 color coordinates of (0.33,0.59).

The LED performance is typically characterized by the wall-plug efficiency (WPE, %), defined by the ratio between the radiant power (W) and the electrical power (W) and by the luminous efficacy (LE, $lm \cdot W^{-1}$), which accounts for the ratio between the luminous flux (lm) and the electric power (W).[23] The WPE was calculated to be 0.25% while the LE for the tU5Tb-derived LED is 1.3 $lm \cdot W^{-1}$. This value is larger than that reported for a β-diketonate $Tb(3Cl\text{-}acac)_3(H_2O)_2$ complex (0.8 $lm \cdot W^{-1}$)[24] indicating that the materials here proposed have the potential to be used as down-shifting phosphors in solid-state lighting. The findings reported here confirm that, with these materials, it is possible to coat UV emitting LEDs, enabling the production of green-emitting LEDs for applications in the traffic light, displays, and human circadian rhythm regulation.

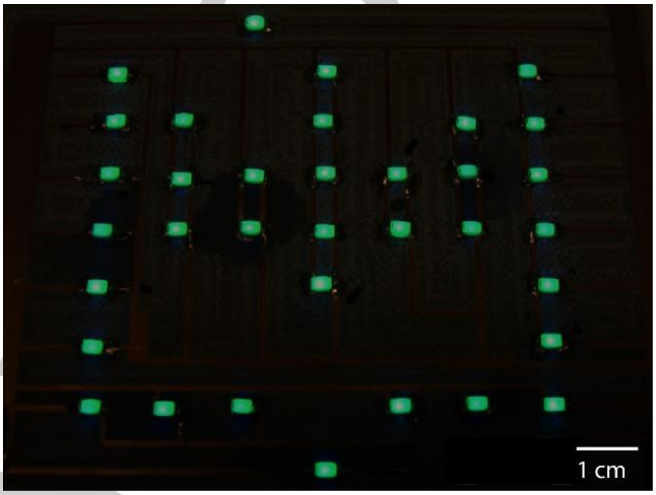


Figure 5. Photograph of the green-emitting LED prototypes: near-UV SMD LEDs (number of LEDs=36) in a printed circuit board and operating at $20\times10^{-3}$ A are coated with tU5Tb.

According to the current state of the art, the higher LE values were reported for inorganic materials such as $Ce^{3+}/Tb^{3+}$co-doped $CaSc_2O_4$ and $Ca_3Sc_2Si_3O_{12}$ [25] hosts both used to coat a UV InGaN LED emitting at 460 nm at $20\times10^{-3}$ A driving current with LE ranging from 7.12 to 27.8 $lm \cdot W^{-1}$. Although the values here reported are lower, we should note, however, that a direct comparison of these values between distinct LEDs must be taken with caution as they depend on the wall-plug efficiency of the UV pumped LED and also on the device geometry. These reported higher efficacy values were also obtained for materials excited in the visible spectral range, which would make them not suitable for use in an RGB phosphor-converted WLED (pcWLEDs).

For a more direct comparison between the fabricated green pcLED and the state of the art, Table 2 shows similar green pcLEDs excited in the near UV range. Depending on the amount of deposited material in the converting layers, the LE can be influenced by the driving current as the material can get saturated by the number of exciting photons that reach it. Therefore, the operation electrical parameters of each one are presented.

**Table 2.** State of the art green pcLED activated by near UV LEDs: emission peak ($\lambda_e$), emission full-width-at-half-maximum (FWHM); excitation wavelength ($\lambda_x$).

| Material | $\lambda_e$ (nm) | FWHM (nm) | Voltage and electrical current | CIE (x,y) | $\lambda_x$ (nm) | LE ($lm \cdot W^{-1}$) |
|---|---|---|---|---|---|---|
| tU5Tb[this work] | ~545 | ~9 | 3.6 V; 20 mA | (0.33,0 .59) | 365 | 1.3 |
| 30TbSal@dU6[7i] | ~543 | <10 | 3.1 V; 44.1 mA | (0.33, 0.61) | 365 | 21.5 |
| $Tb(3Cl\text{-}acac)_3(H_2O)_2$ [24] | ~547 | ~6 | 3.8 V; 20 mA | (0.32,0 .61) | 370 | 0.8 |
| $Ba_5SiO_4(F,Cl)_6:Eu^{2+}$ [26] | ~503 | ~55 | 20 mA | (0.18,0 .43) | 370 | 2.2 |
| $Tb(p\text{-}BBA)_3UA$[27] | ~543 | <10 | 3.6 V; 350 mA | (0.30, 0.62) | 365 | 17.3 |
| $NaCaPO_4:Tb^{3+}$ [27] | ~543 | <10 | 3.6 V; 350 mA | - | 370 | 16.7 |
| $(Ba_{0.46}Sr_{0.46}Eu_{0.08})_3BP_3O_{12}$ [28] | ~505 | ~130 | 350 mA | 0.25, 0.27) | 370 | 5.2 |

The prospects for using tU5Tb as a pcWLED can be further evaluated by comparing its optical parameters to a published simulation[29] where a WLED is made by using RGB components and the ideal characteristics for each RGB component are calculated in order to maximize CRI and LE. Here, it is reported that for a target CRI of 85 and 180 $lm \cdot W^{-1}$ an ideal green would have a dominant wavelength of ~536 nm with FWHM of 34 nm. Comparing these values to the ones in Table 2, the tU5Tb has the closest dominant wavelength to the ideal and the FWHM is estimated to be 9 nm, which points out its applicability for this purpose.

## Conclusions

Green-emitting LEDs were fabricated by coating commercial near-UV-emitting LEDs (365 nm) with photostable UV down-shifting $Tb^{3+}$-activated organic-inorganic hybrids. These hybrid coatings were prepared by the sol-gel method and reveal bright green emission ascribed to the intra-$4f^8$ transition with an intriguing higher emission quantum yield (~0.82). The fabricated prototypes revealed pure CIE color coordinates of (0.33, 0.59) in the green spectral region (~536 nm) and luminous efficacy of ~1.3 $lm \cdot W^{-1}$. These results show that the proposed $Tb^{3+}$-activated materials reveal interesting properties to be used as down-shifting coatings of near-UV emitting LEDs.

## Experimental Section

**Materials.** The chemicals terbium(III) chloride hexahydrate ($TbCl_3.6H_2O$; 99,99%, Sigma-Aldrich), Nalidixic acid (1-ethyl-1,4-dihydro-7-methyl-4-oxo-1,8-naftiridine-3-carboxylic acid, HNal, ≥ 98%, Sigma-Aldrich), sodium hydroxide (NaOH, Merck), Polyoxypropylene (POP) triamine Jeffamine® T5000 (97%, Huntsman) and Polyoxypropylene (POP) triamine Jeffamine® T3000 (97%, Huntsman), 3-isocyanatepropyltriethoxysilane (ICPTES, 95%, Aldrich), tetrahydrofuran (THF, 99.9%, Sigma-Aldrich), ethanol (EtOH, 99.8%, Fluka Riedel-de Haën, and Fisher Scientific), hydrochloric acid (HCl, 37%, Sigma-Aldrich) were used as received. High purity distilled water was used in all experiments.

**Synthetic procedures.** *$Tb(NaI)_3(H_2O)_2$ complex*. For the synthesis of the $Tb(NaI)_3(H_2O)_2$ complex (Figure 1) an amount of 3 mmol of HNaI was dissolved in 10 mL of $CH_3CH_2OH$ and the pH of this solution was adjusted to 6 by adding an appropriate amount of an aqueous NaOH solution (5 % w/v). Then a solution of 1 mmol of $TbCl_3 \cdot 6H_2O$ in 5 mL of water was added dropwise to the ethanolic solution of NaI. The white solid product was filtrated, washed with water and dried in desiccators at room temperature. *Yield:* 80%. Anal Calcd (%) for $C_{36}H_{37}TbN_6O_{11}$: C 48.66, H 4.20, N 9.46. Found C 48.06, H 3.763, N 9.25. ESI–MS m/z (%): 889.2 (100) $[M + H]^+$, 890.3 (40) $[M + H + 1]^+$, 891.3 (11) $[M + H + 2]^+$, For complete details about the general characterization of $Tb(NaI)_3(H_2O)_2$ complex see the Supplementary Information.

*Synthesis of the tri-ureasil hybrid precursors.* Tri-ureasil hybrid material (t-UPTES(5000) and t-UPTES(3000)) are formed from cross-links between the organic and the inorganic components obtained by reacting each of the three -$NH_2$ groups of Jeffamines with the –N=C=O group of ICPTES, in THF, under magnetic stirring at room temperature for 24 h.[14a] The molar ratio of Jeffamine to ICPTES is 1:3. The non-hydrolyzed t-UPTES(5000) and t-UPTES(3000) were obtained as transparent liquids after evaporation under vacuum of THF at room temperature.

*Tri-ureasils doped with $Tb(NaI)_3(H_2O)_2$ complex*. A solution of $Tb(NaI)_3(H_2O)_2$ (5.4 mg, $6 \times 10^{-6}$ mol) in 1 mL of ethanol was left under magnetic stirring for 30 min. This ethanolic solution plus 20 μL of distilled water was added to 1.5 g of the tri-ureasil non-hydrolyzed precursors, t-UPTES(5000) and t-UPTES(3000), under magnetic stirring at room temperature for 15 min. The concentration of $Tb(NaI)_3(H_2O)_2$ complex in the hybrid matrix was 0.069 and 0.071wt% for the t-UPTES(5000) and t-UPTES(3000)-based hybrids, respectively. Then, 40 μL of HCl (0.5 M) were added to catalyze the hydrolysis reactions. Part of the suspension was cast into a polystyrene mold (1.0×1.0×3.0 $cm^3$), covered with Parafilm®, and kept at 40 °C for 48 h. The remaining part of the suspension was used to process thin films deposited on glass substrates (NORMAX, 7.6×2.6×0.1 $cm^3$) by spin-coating at 1000 rpm for 60 s. The films were dried at 40 °C for 24 h, for complete solvent removal.

**UV-down-shifting LED fabrication.** A volume of 10 μL of tU5Tb was deposited by drop cast on the surface of commercial SMD LEDs (UVLED365-SMD, Roithner Lasertechnik GmbH) and left to dry at 45 °C for 48 h. The LEDs emit at 365 nm, with $3 \times 10^{-3}$ W, for forward current value of $20 \times 10^{-3}$ A and applied voltage of 3.6 V. The LEDs were mounted on a PCB board designed (KiCad) to hold 35 LEDs in a parallel circuit, Figure S24. The PCB board was printed using a circuit board plotter (LPKF ProtoMat S103).

**Structural characterization.** Elemental analyses for C, H, N, and S were performed with a CHNS-932 elemental analyzer with standard combustion conditions and handling of the samples in air.

**$^{29}$Si magic-angle spinning (MAS) nuclear magnetic resonance (NMR) and $^{13}$C cross-polarization (CP) MAS NMR spectra:** The $^{29}$Si MAS NMR

spectra were recorded with a Bruker III Avance 400 and Bruker III Avance 500 (9.4 T) spectrometer at 79.49 and 100.62 MHz, respectively. $^{29}$Si MAS NMR spectra were recorded with 2 µs (~ 30 °) rf pulses, a recycle delay of 60 s and at a 5.0 kHz spinning rate. The $^{13}$C CP/MAS NMR spectra were recorded with 4 µs 1H 90 ° pulses, 2 ms contact time, a recycle delay of 4 s and at a spinning rate of 8 kHz. Chemical shifts (δ) are quoted in ppm from TMS. Further details in the Supplementary Information.

**Electrospray mass spectrometry (ESI–MS).** The ESI-MS experiments were performed using an ion trap mass spectrometer (LCQ Duo from Thermo Finnigan). Samples were dissolved in methanol and introduced by an infusion pump at a flow rate of 500 µL $h^{-1}$. The applied spray potential was 4.5 kV and the capillary temperature was set at 200 °C. All remaining parameters were optimized to ensure the highest abundance possible for the ions of interest. MS data were acquired in the positive ion mode.

**Fourier transform infrared (FT-IR)**. The FT-IR spectra were obtained as KBr pellets using a MATTSON 7000 FTIR Spectrometer. The spectra were collected in the 350-4000 $cm^{-1}$ range by averaging 256 scans at a spectral resolution of 2 $cm^{-1}$. Attenuated total reflectance (ATR) FT-IR spectra were measured on the MATTSON 7000 FTIR Spectrometer instrument equipped with a Specac Golden Gate Mk II ATR accessory having a diamond top-plate and KRS-5 focusing lenses.

**Fourier-transform (FT) Raman spectroscopy.** The FT-Raman spectra were recorded on an FT Bruker RFS-100 spectrometer using a Nd:YAG laser (Coherent Compass-1064/500N) with an excitation wavelength of 1064 nm. The spectra were collected in the 150-4000 $cm^{-1}$ range at a spectral resolution of 2 $cm^{-1}$.

**Optical characterization.** UV/visible absorption spectra were measured using a Lambda 950 dual-beam spectrometer (Perkin-Elmer).The photoluminescence spectra were recorded at 18 K and 300 K with a Horiba Scientific modular double grating excitation spectrofluorimeter and a TRIAX 320 emission monochromator (Fluorolog-3) coupled to an R928 Hamamatsu photomultiplier, using front face acquisition mode. The excitation source was a 450 W Xe arc lamp. The emission spectra were corrected for detection and the optical spectral response of the spectrofluorimeter and the excitation spectra were corrected for the spectral distribution of the lamp intensity using a photodiode reference detector. Emission decay curves were recorded on a Fluorolog TCSPC spectrofluorometer coupled to a TBX-04 photomultiplier tube module (950 V), 200 ns time to-amplitude converter and 70 ns delay using a Horiba Scientific pulsed diode (SpectraLED-355, peak at 356 nm) as the excitation source. Both photoluminescence spectra and lifetime measurements were performed in solid-state. Room temperature emission quantum yield measurements were obtained by using a Hamamatsu C9920-02 setup with a 150 W Xe lamp coupled to a monochromator for wavelength discrimination, an integration sphere as sample chamber and a multichannel analyzer for signal detection. Three measurements were made for each sample and the average values obtained are reported with accuracy within 10% according to the manufacturer. The LED performance was evaluated during 24 h under continuous operation at 3.378 V. The radiant flux (W) and the luminous flux ($lm \cdot W^{-1}$) of the LED were measured using an integrating sphere ISP 150L-131, Instrument Systems. The integrating sphere ($BaSO_4$ coating) has internal diameter of 150 mm and was coupled to an array spectrometer MAS 40 from Instrument Systems. The measurements are accurate within 5%, according to the manufacturer.

## Acknowledgments

This work was developed within the scope of the project CICECO-Aveiro Institute of Materials (UIDB/50011/2020 & UIDP/50011/2020) and WINLEDs (POCI-01-0145-FEDER-030351) financed by national funds through the Fundação para a Ciência e a Tecnologia/Ministério da Educação e Ciência (FCT/MEC) and co-financed by FEDER under the PT2020 Partnership Agreement. The NMR spectrometers are part of the National NMR Network (PTNMR) and are partially supported by Infrastructure Project Nº 022161 (co-financed by FEDER through COMPETE 2020, POCI and PORL and FCT through PIDDAC). SFHC thanks SolarFlex, CENTRO-01-0145-FEDER-030186. FCT is gratefully acknowledged for funding a researcher contract to MMN (IF/01468/2015). Instituto de Telecomunicações from University of Aveiro is acknowledged for the PCB printing and RR Rondão from University of Aveiro is acknowledged for the hybrids' synthesis.

**Keywords:** green light-emitting diodes • lanthanides • near-UV light-emitting diodes • organic-inorganic hybrids• solid-state lighting

[1] A. de Almeida, B. Santos, B. Paolo, M. Quicheron, *Renew. Sust. Energ. Rev.* **2014**, *34*, 30-48.
[2] X. B. Luo, R. Hu, S. Liu, K. Wang, *Prog. Energ. Combust.* **2016**, *56*, 1-32.
[3] J. McKittrick, L. E. Shea-Rohwer, *J. Am. Ceram. Soc.* **2014**, *97*, 1327-1352.
[4] N. C. George, K. A. Denault, R. Seshadri, *Annu. Rev. Mater. Res.* **2013**, *43*, 481-501.
[5] R. A. Oliver, *Mater. Sci. Tech.-Lond.* **2016**, *32*, 737-745.
[6] J. J. D. McKendry, D. Massoubre, S. L. Zhang, B. R. Rae, R. P. Green, E. Gu, R. K. Henderson, A. E. Kelly, M. D. Dawson, *J. Lightwave Technol.* **2012**, *30*, 61-67.
[7] a) A. E. Stapleton, *Plant Cell* **1992**, *4*, 1353-1358; b) R. M. Klein, *Biol. Rev.* **1992**, *67*, 199-284; c) T. A. LeGates, D. C. Fernandez, S. Hattar, *Nat. Rev. Neurosci.* **2014**, *15*, 443-454; d) N. Yeh, P. Yeh, N. Sh'ih, O. Byadgi, T. C. Cheng, *Renew. Sust. Energ. Rev.* **2014**, *32*, 611-618; e) A. Wunsch, K. Matuschka, *Photomed. Laser Surg.* **2014**, *32*, 93-100; f) M. C. Snowden, K. R. Cope, B. Bugbee, *PLoS One* **2016**, *11*, e0163121; g) P. M. Pattison, J. Y. Tsao, G. C. Brainard, B. Bugbee, *Nature* **2018**, *563*, 493-500; h) D. C. Negelspach, S. Kaladchibachi, F. Fernandez, *Proc. R. Soc. B* **2018**, *285*, 20181288; i) M. Fang, A. G. Bispo-Jr, L. Fu, R. A. S. Ferreira, L. D. Carlos, *J. Lumin.* **2020**, *219*, 116910.
[8] B. N. Ding, *Mater. Sci. Tech.* **2018**, *34*, 1615-1630.
[9] P. F. Smet, A. B. Parmentier, D. Poelman, *J. Electrochem.Soc.* **2011**, *158*, R37-R54.
[10] N. Sabbatini, M. Guardigli, J. M. Lehn, *Coordin. Chem. Rev.* **1993**, *123*, 201-228.
[11] a) H. Uh, S. Petoud, *CR Chim.* **2010**, *13*, 668-680; b) S. I. Weissman, *J. Chem. Phys.* **1942**, *10*, 214-217.
[12] S. V. Eliseeva, V. S. Liasotkyi, I. P. Golovach, P. G. Doga, V. P. Antonovich, S. Petoud, S. B. Meshkova, *Methods Appl. Fluores.* **2017**, *5*, 014002.
[13] a) V. T. Freitas, P. P. Lima, R. A. S. Ferreira, E. Pecoraro, M. Fernandes, V. de Zea Bermudez, L. D. Carlos, *J. Sol-Gel Sci. Techn.* **2013**, *65*, 83-92; b) S. F. H. Correia, P. P. Lima, E. Pecoraro, S. J. L. Ribeiro, P. S. Andre, R. A. S. Ferreira, L. D. Carlos, *Prog. Photovolt.: Res. Appl.* **2016**, *24*, 1178-1193.
[14] a) V. T. Freitas, P. P. Lima, V. de Zea Bermudez, R. A. S. Ferreira, L. D. Carlos, *Eur. J. Inorg. Chem.* **2012**, *2012*, 5390-5395; b) V. T. Freitas, P. P. Lima, R. A. S. Ferreira, L. D. Carlos, E. Pecoraro, S. J. L. Ribeiro, V. de Zea Bermudez, *J. Sol-Gel Sci. Techn.* **2014**, *70*, 227-235; c) L. D. Carlos, R. A. S. Ferreira, V. de Zea Bermudez, S. J. L. Ribeiro, *Adv. Funct. Mater.* **2001**, *11*, 111-115.
[15] V. de Zea Bermudez, L. D. Carlos, L. Alcácer, *Chem. Mater.* **1999**, *11*, 569-580.
[16] L. D. Carlos, V. de Zea Bermudez, R. A. S. Ferreira, L. Marques, M. Assunção, *Chem. Mater.* **1999**, *11*, 581-588.
[17] N. Willis-Fox, A. T. Marques, J. Arlt, U. Scherf, L. D. Carlos, H. D. Burrows, R. C. Evans, *Chem. Sci.* **2015**, *6*, 7227-7237.

[18] a) E. Pecoraro, R. A. S. Ferreira, C. Molina, S. J. L. Ribeiro, Y. Messsaddeq, L. D. Carlos, *J. Alloy. Compd.* **2008**, *451*, 136-139; b) J. Graffion, X. Cattoen, M. W. C. Man, V. R. Fernandes, P. S. Andre, R. A. S. Ferreira, L. D. Carlos, *Chem. Mater.* **2011**, *23*, 4773-4782.

[19] P. P. Lima, S. S. Nobre, R. O. Freire, S. A. Junior, R. A. S. Ferreira, U. Pischel, O. L. Malta, L. D. Carlos, *J. Phys. Chem. C* **2007**, *111*, 17627-17634.

[20] E. Mamontova, J. Long, R. A. S. Ferreira, A. M. P. Botas, F. Salles, Y. Guari, L. D. Carlos, J. Larionova, *Nanoscale* **2019**, *11*, 7097-7101.

[21] C. Molina, K. Dahmouche, Y. Messaddeq, S. J. L. Ribeiro, M. A. P. Silva, V. de Zea Bermudez, L. D. Carlos, *J. Lumin.* **2003**, *104*, 93-101.

[22] L. D. Carlos, R. A. S. Ferreira, V. de Zea Bermudez, S. J. L. Ribeiro, *Adv. Mater.* **2009**, *21*, 509-534.

[23] X. Bai, G. Caputo, Z. Hao, V. T. Freitas, J. Zhang, R. L. Longo, O. L. Malta, R. A. S. Ferreira, N. Pinna, *Nat. Commun.* **2014**, *5*, 5702.

[24] M. M. Nolasco, P. M. Vaz, P. D. Vaz, R. A. S. Ferreira, P. P. Lima, L. D. Carlos, *J. Coord. Chem.* **2014**, *67*, 4076-4089.

[25] a) Y. B. Chen, K. W. Cheah, M. L. Gong, *J. Lumin.* **2011**, *131*, 1589-1593; b) Y. B. Chen, K. W. Cheah, M. L. Gong, *J. Lumin.* **2011**, *131*, 1770-1775; c) Y. B. Chen, M. L. Gong, K. W. Cheah, *Mater. Sci. Eng. B-Adv.* **2010**, *166*, 24-27.

[26] X. G. Zhang, X. X. Wang, J. Q. Huang, J. X. Shi, M. L. Gong, *Opt. Mater.* **2009**, *32*, 75-78.

[27] N. Q. Sun, L. P. Li, Y. M. Yang, A. Q. Zhang, H. S. Jia, X. G. Liu, B. S. Xu, *Opt. Mater.* **2015**, *49*, 39-45.

[28] T. W. Kuo, W. R. Liu, T. M. Chen, *Opt. Express* **2010**, *18*, 1888-1897.

[29] M. S. Xu, H. X. Zhang, Q. B. Zhou, H. Wang, *Appl. Optics* **2016**, *55*, 4456-4460.

**Entry for the Table of Contents** (Please choose one layout)

Layout 1:

FULL PAPER

Green-emitting LEDs were fabricated by coating commercial near-UV-emitting LEDs (365 nm) with high emission quantum yield (~0.82) and photostable UV down-shifting $Tb^{3+}$-activated organic-inorganic hybrids prepared by the sol-gel method. The fabricated devices revealed pure CIE colour coordinates in the green spectral region and luminous efficacy of ~1.3 $lm \cdot W^{-1}$.

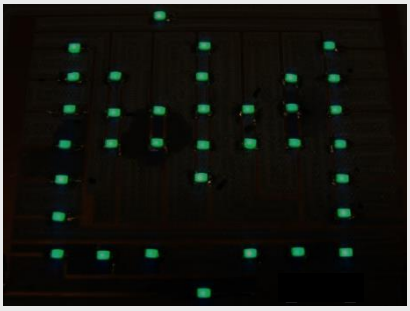

**Green-emitting LED**

*Sandra F. H. Correia, Ricardo L. Fernandes, Lianshe Fu, Mariela M. Nolasco, Luís D. Carlos, Rute A. S. Ferreira**

***Page No. – Page No.***

**High emission quantum yield $Tb^{3+}$-activated organic-inorganic hybrids for UV-down shifting green light emitting diodes**

*one or two words that highlight the emphasis of the paper or the field of the study

Layout 2:

FULL PAPER

((Insert TOC Graphic here; max. width: 11.5 cm; max. height: 2.5 cm; NOTE: the final letter height should not be less than 2 mm.))

Text for Table of Contents (about 350 characters)

**Key Topic***

*Author(s), Corresponding Author(s)**

***Page No. – Page No.***

**Title**

*one or two words that highlight the emphasis of the paper or the field of the study